RSCPublishing **Analyst**

Rapid recognition of drug-resistance/sensitivity in leukemic cells by Fourier transform InfraRed microspectroscopy and unsupervised Hierarchical Cluster Analysis.

Journal Name

Analyst

ARTICLE TYPE

Rapid recognition of drug-resistance/sensitivity in leukemic cells by Fourier transform InfraRed microspectroscopy and unsupervised Hierarchical Cluster Analysis.

Giuseppe Bellisola,[*a,b] **Gianfelice Cinque,** [*c] **Marzia Vezzalini,** [*b] **Elisabetta Moratti,**[b] **Giovannino**
5 **Silvestri,**[b] **Sara Redaelli,** [*d] **Carlo Gambacorti Passerini,**[d] **Katia Wehbe,** [*c] **and Claudio Sorio**[*b]

We tested the ability of Fourier Transform (FT) InfraRed (IR) microspectroscopy (microFTIR) in combination with unsupervised Hierarchical Cluster Analysis (HCA) in identifying drug-
10 resistance/sensitivity in leukemic cells exposed to tyrosine kinase inhibitors (TKIs). Experiments were carried out in a well established mouse model of human Chronic Myelogenous Leukemia (CML). Mouse-derived pro-B Ba/F3 cells transfected with and stably expressing the human p210$^{BCR-ABL}$ drug-sensitive wild-type *BCR-ABL* or the V299L or T315I p210$^{BCR-ABL}$ drug-resistant *BCR-ABL* mutants were separately exposed to imatinib-mesylate (IMA) or dasatinib (DAS). MicroFTIR was carried out at the Diamond IR
15 beamline MIRIAM where the mid-IR absorbance spectra of individual Ba/F3 cells were acquired using the high brilliance IR synchrotron radiation (SR) via aperture of 15x15 μm^2 in sizes. Conventional IR source (globar) was used to compare average spectra over 15 cells or more. IR signatures of drug actions were identified by supervised analyses in the spectra of TKIs-sensitive cells. Unsupervised HCA applied to selected intervals of wavenumber allowed to classify the IR patterns of viable (drug-resistant) and
20 apoptotic (drug-sensitive) cells with an accuracy >95%. The results from microFTIR+HCA analysis were cross-validated with those obtained via immunochemical methods, *i.e.* immunoblotting and flow cytometry (FC) that resulted directly and significantly correlated. We conclude that this combined microFTIR+HCA method potentially represents a rapid, convenient and robust screening approach to study the impact of drugs in leukemic cells included peripheral blasts from patients in clinical trials with
25 new anti-leukemic drugs.

Introduction

Increasing knowledge on the molecular pathogenesis of chronic myelogenous leukemia (CML) has resulted in the development of new therapeutic molecules able to improve the outcome in CML
30 patients.[1]

Imatinib-mesylate (IMA) is the prototype compound of tyrosine kinase inhibitors (TKIs) targeting the abnormal tyrosine kinase (TK) activity associated to the kinase domain (KD) of Bcr-Abl oncoproteins (p190, p210, or p230 kDa, respectively). Bcr-
35 Abl is the product of the *BCR-ABL* chimeric fusion gene (the Philadelphia chromosome, Ph$^+$) derived from a reciprocal translocation between the breakpoint cluster region (*BCR*) gene located on chromosomes 22 and the *c-Abl* gene (*ABL*) located on chromosome 9 in the multi-potent bone marrow stem cell. The
40 presence of Ph$^+$ in CML cells confers growth factor independence and resistance to apoptosis allowing the progressive expansion of leukemic cell populations in the bone marrow during chronic phase.[2] IMA has proved to be effective in inducing hematologic and cytogenetic remission in most CML patients. Unfortunately,
45 a significant percentage of them tend to develop both primary and secondary resistance to IMA often leading to treatment failure.

The clinical transition from chronic to blast phase is characterised by the high numbers of CML blast cells with additional changes in the Bcr-Abl KD that circulate in the blood of those patients and
50 associate with more clinically aggressive and drug-resistant phenotypes.[3] Second-third generation TKIs such as Dasatinib (DAS),[4] nilotinib,[5] and bosutinib[6] have activity against many Bcr-Abl mutants except T315I mutation for which new drug molecules are in the development pipeline. [7,8]
55 Most popular molecular predictors of drug response in CML patients are the *BCR-ABL* transcript levels measured by real-time quantitative PCR, the Bcr-Abl KD mutation analysis, and the monitoring of Bcr-Abl activity.[9-12] Major drawbacks are the poor standardisation and high costs of molecular methods for
60 monitoring patients. Sometime genome expression profiling is unable to identify reproducible signatures of drugs and/or to predict drug-resistance in CML patients.[13] Therefore, it is of great interest the development of new reliable and cost-effective methods to obtain rapid and accurate information on the
65 sensitivity of CML cells to TKIs.

The present work aims at exploring whether Fourier transform (FT) infrared (IR) microspectroscopy (microFTIR) in

combination with methods for pattern recognition, *i.e.* unsupervised hierarchical cluster analysis (HCA), could represent a new and convenient analytical approach to obtain information on the sensitivity and resistance of CML cells to TKIs.

5 MicroFTIR has the advantages of being a non-destructive, higly sensitive and specific analytical technique to detect molecular changes. In a few seconds it provides specific and spatially resolved biochemical information about molecular constituents within individual cells.[14,15] In association with advanced

10 chemometrics methods, microFTIR has already shown potential applications in histopathology, cell biology, and cell pharmacology.[16-23]

Methods

Ba/F3 cells

15 Experiments with TKIs were carried out in a well established mouse-derived Ba/F3 cell model of human Ph[+] CML consisting of drug-sensitive cells and drug-resistant mutants.[24]

Mouse pro-B Ba/F3 cells (parental, par-Ba/F3) transfected with and stably expressing the human p210[BCR-ABL] drug-sensitive

20 wild-type *BCR-ABL* (wt-Ba/F3) or the V299L or T315I p210[BCR-ABL] drug-resistant *BCR-ABL* mutants (V299L- and T315I-Ba/F3, respectively) were grown under sterile conditions in a humidified atmosphere with 5% CO_2 and in RPMI 1640 medium added with 2 mmol L^{-1} L-glutamine, 10% foetal bovine serum (FBS), and no

25 antibiotic. Parental Ba/F3 was the *BCR-ABL* negative control cell line used to test the non specific toxicity of TKIs. WEHI-B3 conditioned supernatant was added to the RPMI medium (10% v/v) as a source for interleukin 3 (IL-3) which is necessary to grow par-Ba/F3.[25] Wild-type Ba/F3 cells and V299L- and T315I-

30 Ba/F3 cell mutants were selected and expanded in RPMI medium with no IL-3. Wild-type Ba/F3 cells are sensitive to the pro-apoptotic actions of both IMA and DAS. The V299L-Ba/F3 cell mutant is sensitive to IMA and resistant to DAS, whereas T315I-Ba/F3 cell mutant is resistant both to IMA and DAS, respectively.

35 **Tyrosine Kinase Inhibitors (TKIs)**

Imatinib-mesylate (IMA) is the 4-[(4-methylpiperazin-1-yl)methyl]-N-[4-methyl-3-[(4-pyridin-3-ylpyrimidin-2yl)amino]-phenyl]-benzamide compound, also known as CGP057148B and STI571 from Novartis Pharma AG, Basel.[26] IMA was dissolved

40 (w/v) in sterile H_2O to obtain a 10 mmol L^{-1} IMA stock solution that is stable at -20°C and in the dark for some weeks. Blocking the binding of ATP to the KD of Bcr-Abl, IMA inhibits the associated TK activity, restores the sensitivity of CML cells to pro-apoptotic factors and induces cell apoptosis.

45 Dasatinib (DAS), from Bristol-Myers Squibb BMS-354825 (N-(2-chloro-6-methylphenyl)-2-[[6-[4-(2-hydroxyethyl)-1-piperazinyl]-2-methyl-4-pyrimidinyl]amino]-5-thiazole carboxamide monohydrate, is a dual-specific inhibitor of Src and of both active and inactive conformations of Abl.[27] DAS (17.2

50 mg) was dissolved in 1 mL DMSO to obtain a 35.2 mM DAS stock solution and aliquots were stored at -20°C.

In time-course experiments with TKIs, 2.5×10^6 Ba/F3 cells and mutants suspended in 1.5 mL RPMI medium were separately exposed for 24 or 48 hours to 2.0 μM IMA or 16.0 nM DAS,

55 respectively. Appropriate control samples (CTRLs) with no added drug or with DMSO diluted in the growth medium (v/v

1/2000) as in DAS-treated samples were also prepared. All experiments were performed at least in triplicate.

Sample preparation.

60 At the end of incubation, a volume of 0.5 mL of 4% buffered-paraformaldehyde (PFA) solution was added to 1.5 mL Ba/F3 cells suspension. Cells were fixed in 1% PFA for at least 30 min., pelleted by centrifugation (65g for 2 min.) and re-suspended twice in H_2O. A drop (10 μL) of each cell suspension was

65 carefully deposited and air-dried on 50x25x2 mm ZnSe polished crystal to obtain an array of sample spots with cells spread in monolayer (ESI: Fig. S1).[28]

FTIR absorbance microspectroscopy (microFTIR).

The IR absorbance spectra were acquired at Diamond Light

70 Source (DLS, UK) at the B22 IR beamline Multiband Infrared Imaging and Microspectroscopy (MIRIAM).[29] Two IR sources were used: the highest brilliance synchrotron radiation (SR) for single cell analysis and the globar for average measurements on larger areas. In both cases the mid-IR spectral region between

75 4000 cm^{-1} and 400 cm^{-1} was used.

In a typical SR microFTIR experimental setting in transmission modality, we used the Bruker 80V interferometer coupled with a Hyperion 3000 Vis-IR microscope equipped with 36x magnification objective (N.A. 0.6) and identical condenser

80 optics; a high sensitivity liquid nitrogen cooled Mercury-Cadmium-Telluride (MCT) detector was used in combination with a Ge filter. To acquire the IR absorbance spectra of individual cells, samples were positioned under the objective and the four blade slits of the microscope were restricted to aperture

85 values of 15x15 $μm^2$ fitting the sizes of a cell (diameter 12-15 μm). To optimize microFTIR performed with the broadband globar as more conventional IR source, the average absorbance spectra representative of about 15-20 cells were acquired from several areas of 50x50 $μm^2$ in sizes within the sample and IR

90 signals were collected. To obtain the necessary signal to noise ratio (S/N) in the spectra a number of 256 scans by scanner velocity of 40 kHz were performed in continuous mode at spectral resolution of 4 cm^{-1} both on the sample and the background (clean ZnSe substrate area). This is equivalent to a

95 spectrum within 60 seconds.

Pre-processing

Using different functions in OPUS™ 6.5 software (Bruker Optik GmbH, Ettlingen, Germany), atmospheric and water vapour interferences were compensated and background intensity

100 changes were corrected (concave rubberband correction) within the selected 3800-800 cm^{-1} interval of wavenumbers (wnrs). To minimize the effects of different thickness within sample and among samples, spectra were pre-processed with vector normalization function and the second derivative spectra were

105 calculated with a simultaneous smoothing based on Savitzky-Golay algorithm on 9 smoothing points. Signal to noise ratio (S/N) was systematically calculated as transmission signal versus root mean square value of the noise within the 2600-2400 cm^{-1} interval.

110 **Supervised analyses**

Number, position and shape of marker peaks were identified and

compared in the spectra. The position of two peaks was considered significantly shifted when the difference exceeded the value of spectral resolution (>4 cm^{-1}). The second order derivative was analysed in corresponding absorbance spectra to identify band and sub-band components within marker peaks. They were assigned according to the *so called* group frequency approach which associates the absorbance of specific functional groups in molecules with well defined vibrational frequencies reported in the literature.[30] In quantitative analysis we compared the mean values of integral calculated by drawing a straight line between the two frequency limits delimiting the selected marker peak/region.

Unsupervised Hierarchical Cluster Analysis (HCA)

In hierarchical cluster analysis (HCA) with no assumption, one or more sub-regions within the spectra of a dataset are input to a clustering algorithm that pools them into groups based solely on their similarity to one other. Although the number of groups and the criterion by which similarity is defined (*i.e.*, Euclidean distance) must be chosen, the resulting output is a non-subjective grouping of the spectra.[31]

HCA was applied to one or more selected intervals of wnrs in the FTIR spectra pre-processed with vector normalization and second derivative. Typically, the 1760-1480 cm^{-1} interval was selected to recognize the IR pattern of viable and apoptotic cells whereas the 1150-900 cm^{-1} interval was used to group the spectra according to changes in phosphate signals, respectively. Initially, a standard method merging two spectra with the smallest spectral distance into a cluster was applied to calculate Euclidean distances among the spectra of individual cells. Then, Ward's algorithm calculated spectral distances between this newly-created cluster and all the other spectra or clusters. All spectra grouped in each of the two final classes with the highest heterogeneity value were averaged to obtain the representative spectrum of corresponding final class.[32]

Independent cross-validation of IR data analyses

We applied immunomethods to measure the degrees of protein phosphorylation and apoptotic processes in Ba/F3 cells of replicate samples. The results were compared with those obtained from IR analyses in the spectra.[28]

The expression of Bcr-Abl and the degrees of protein phosphotyrosine were studied in Ba/F3 cell lysates adjusted to 1.0 mg total protein mL^{-1}. Samples (20 µL) were separated on 10% acrylamide/bisacrylamide gel, electroblotted on polyvinylidene difluoride (PVDF) membranes and probed with a mixture of 4G10 and PY99 anti-phosphotyrosine antibodies (from Upstate Biotechnology, Waltham, and Santa Cruz Biotechnology, Santa Cruz, USA, respectively). After a second incubation with HRP conjugated secondary antibodies, the complex was visualized by enhanced chemi-luminescence (ECL detection system, Amersham, NJ, USA). After stripping, PVDF membrane was incubated with anti-c-Abl sc-887 (Santa Cruz Biotechnology, Santa Cruz, USA) probing Bcr-Abl and anti-actin as a control of constitutive protein expression in cells.

The mean percentages of viable and apoptotic Ba/F3 cells were determined by flow cytometric (FC) analysis of fluorescence in cells stained with e-Fluor 450 for Annexin-V (eBioscience, Inc. San Diego, CA, USA) and Propidium Iodide (PI) vital dye as

previously reported.[28] The unsupervised pattern recognition approach resulted cross-validated when the results of HCA and FC analyses were in agreement.

Statistics

According to results distribution, parametric and/or non parametric statistics were applied to test hypotheses on the means and/or the medians, respectively. The α value was set to 0.05 and the level of significant difference to $P < 0.05$.

Results

Representative FTIR absorbance spectra of untreated CTRLs (blue traces) and of Ba/F3 cells and mutants exposed for 48 hours to 2.0 µM IMA (red traces) are shown in Fig. 1, respectively. Some differences between wt- and V299L-Ba/F3 cells exposed to IMA and corresponding untreated CTRLs can be immediately appreciated within the 1760-1480 cm^{-1} and 1150-900 cm^{-1} interval. Opposite, the spectra of Bcr-Abl negative par-Ba/F3 cells and of drug-resistant Bcr-Abl mutant T315I-Ba/F3 exposed to IMA are very similar to those of their untreated CTRLs.

Marker peaks within the 3000-2800 cm^{-1} interval in Fig. 1A mainly reflect the N-H stretching vibration of protein amide A (v_{max}3290 cm^{-1}) and amide B (v_{max}3060 cm^{-1}), and the anti-symmetric and symmetric C-H stretching vibration from CH$_3$ (v_{max}2956 cm^{-1} and v_{max}2872 cm^{-1}) and CH$_2$ (v_{max}2925 cm^{-1} and v_{max}2853 cm^{-1}) groups in lipids, respectively. Within the 1800-900 cm^{-1} interval (Fig. 1B) we identified and assigned the following spectral components according to the data published in the literature.[33-35] The shoulder at v_{max}1740 cm^{-1} was mainly assigned to the C=O stretching vibration of esters in membrane phospholipids although it can also reflect changes in the protonation of aspartic and glutamic acid. The most prominent peaks within the 1700-1480 cm^{-1} interval mainly reflect the absorbance of amide I (v_{max}1650 cm^{-1}) and amide II (v_{max}1540 cm^{-1}) in proteins, respectively. The region of amides is sensitive either to the hydration level in sample and to changes in the secondary structures of proteins. Purging samples with nitrogen minimised the variability related to the hydration level in samples as well as the interference of free water was subtracted from the spectra by an appropriate algorithm allowing to compare changes in the secondary structures of proteins among samples. In particular, α-helical structures contribute with a component at v_{max}1650 cm^{-1}, aggregated β-sheet structures absorb at v_{max}1628 cm^{-1}, and tyrosine residues in proteins have a components at v_{max}1512 cm^{-1}. The anti-symmetric scissoring of CH$_3$ in lipids and proteins and the C=O stretching vibrations of COO- in fatty acids and amino acid side chain absorb at v_{max}1450 cm^{-1} and at v_{max}1400 cm^{-1}, respectively. The two major absorbance peaks within the 1300-1000 cm^{-1} interval originate from the anti-symmetric (v_{max}1240 cm^{-1}) and symmetric (v_{max}1086 cm^{-1}) stretching of PO$_2^-$ groups in nucleic acids DNA and RNA. However, also other phosphate groups such as COP in phospholipids (v_{max}1086 cm^{-1}) as well as the vibrations of applied to the 1760-1480 cm^{-1} and 1150-900 cm^{-1} intervals CH$_2$OH groups (v_{max}1056 cm^{-1}) and of COH groups (v_{max}1020 cm^{-1}) in carbohydrates may contribute to the shape of marker peak with limits 1140-990 cm^{-1}. The stretching vibrations of CC and CO functional groups in the deoxyribose and phosphate moieties of
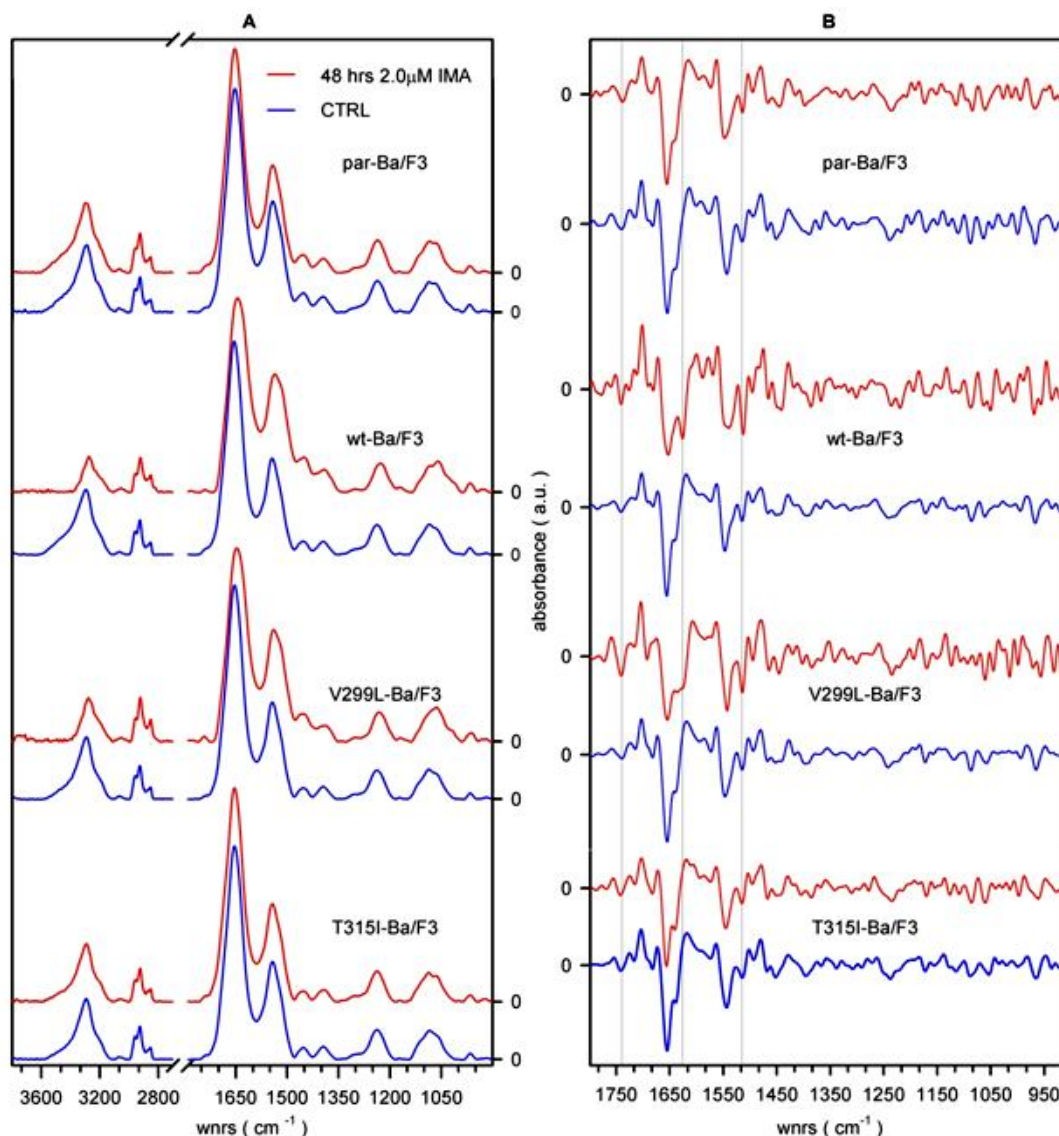
ARTICLE TYPE

Fig. 1 Supervised analyses in the representative FTIR absorbance spectra of mouse-derived Ba/F3 cells model of human chronic myeloid leukemia (CML). A. Normalized and baseline corrected spectra are shown within the 3800-800 cm^{-1} interval of wnrs (omitted 2700-1800 cm^{-1} interval). Blue traces: untreated control (CTRL); red traces: samples exposed to 2.0 μM imatinib mesylate (IMA) for 48 hours. B. The corresponding second order derivative spectra within the 1800-900 cm^{-1} interval. Typical IR signatures of cell apoptosis induced by IMA have been marked with grey lines.

DNA backbone have been reported to occur also at $v_{max}965$ cm^{-1} whereas the small peaks at $v_{max}950$ cm^{-1} and at $v_{max}915$ cm^{-1} have been assigned also to the absorbance of PO_3^{2-} in phosphorylated proteins. Although the univocal interpretation of pre-assigned IR signals cannot be always obtained, the 1800-900 cm^{-1} interval is generally considered as a "fingerprinting" useful to classify the pattern of individual cells by the means of appropriate algorithms.

We optimised microFTIR setup in order to achieve appropriate signal to noise (S/N) values in the spectra at the necessary spatial resolution. In fact, the high flux of IR photons released at the sample plane by the narrowed beam from the highest brilliance SR IR source is within the MCT detector dynamic range and enhances the IR signals from the cell restricted within 15x15 μm^2 (or lower) aperture slits well above the background noise. Therefore, the S/N value in the SR spectrum results appropriate (S/N = 6500). On the contrary, over the same sample area by the isotropic and broad globar source, lower S/N values are achieved in the spectrum (S/N = 1300) as expected (ESI: Fig. S1). Lower S/N values increase the uncertainty in revealing thus assigning bands and sub-bands, *i.e.*, within the region of phosphate signals, and reduce also the probability to classify spectra by unsupervised HCA correctly. Considering that globar is the

conventional IR source for routine applications we optimised microFTIR using a broadband MCT setting the aperture slits of the microscope to delimit spot areas of 50x50 μm^2 in sizes. Over homogeneous zones of the sample (Fig. S1), we could obtain

5 spectra of quality similar to those of individual cells by SR microFTIR. IR signals could be identified and assigned by supervised method within and unsupervised HCA applied to the 1300-900 cm^{-1} interval of wnrs (Fig. S1, middle).
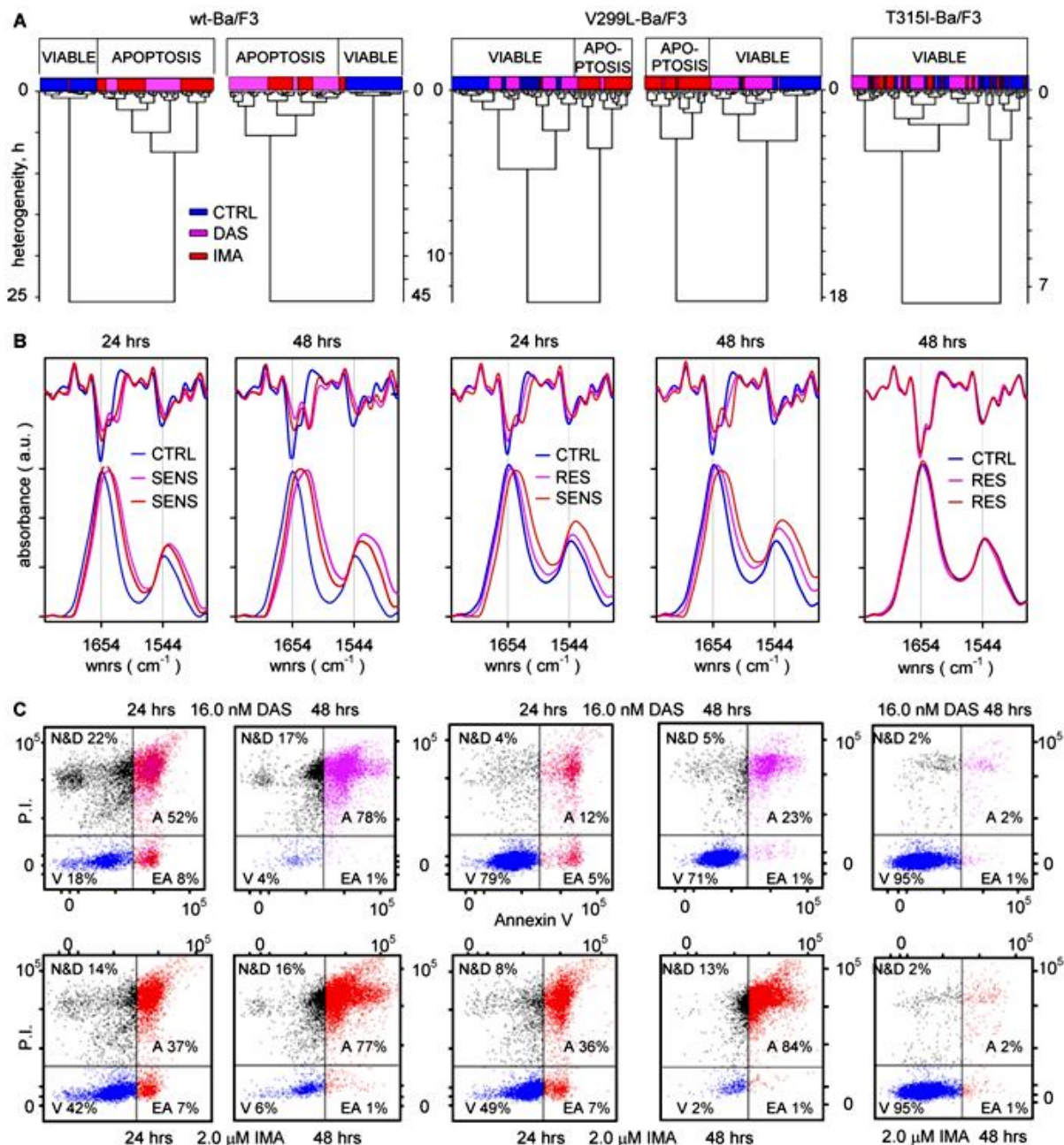

10 **Fig. 2** Unsupervised recognition of IR patterns by hierarchical cluster analysis (HCA). A. HCA was applied to the 1760-1480 cm^{-1} interval of SR FTIR absorbance spectra of individual cells in untreated CTRL, and DAS- or IMA-treated (24 or 48 hours) samples of wt-, V299L-, and T315I-Ba/F3 cells (24 hrs has been omitted). B. The representative spectra averaging those of individual cells grouped in each of the two final classes are shown according to the condition of drug treatment: blue, untreated CTRL; pink, 16.0 nm DAS; red, 2.0 µM IMA. The corresponding second derivatives have been superimposed to highlight spectral differences between drug-sensitive (SENS) and drug-resistant (RES) cells as compared to those of untreated CTRL (blue). C. The
15 cross-validation of HCA by flow cytometry (FC). Dot-plots of Annexin-V to Propidium Iodide (P.I.) staining in Ba/F3 cells and mutants exposed to 16.0 nM DAS or 2.0 µM IMA for 24 and 48 hours, respectively. The relative percentages of viable cells (V), of cells in early and late apoptosis (EA, A, respectively), and of necrotic cells and debris (N&D) measured in a typical time-course experiment with drugs have been reported.

Supervised identification of IR markers of TKIs interference with cell growth processes

20 Using the supervised group frequency approach we recognised some typical IR signatures related to apoptotic processes in

cells.[28,36-42] As compared to untreated CTRL (blue traces in Fig. 1), the peaks of amide I and amide II are significantly shifted towards lower wnrs in the absorbance spectra of drug-sensitive 25 Ba/F3 cells and mutants exposed to IMA (red traces of wt- and

V299L-Ba/F3 cells in Fig. 1, respectively) whereas they coincide in the spectra of drug-resistant cells (red traces of par- and T315I-Ba/F3 cells in Fig. 1). Vibrational changes are more evident in the second derivative spectra (Fig. 1B) where both the decreased absorbance of component assigned to α-helical structures (v_{max}1650 cm^{-1}) and the increased absorbance of component assigned to aggregated β-sheet structures (v_{max}1628 cm^{-1}) contribute to the shift of amide I normally peaking at v_{max}1650 cm^{-1} in untreated CTRL towards v_{max}1640 cm^{-1} (or lower) wnrs in the spectra of apoptotic cells, respectively. In a similar manner, the increased absorbance of component assigned to tyrosine residues in proteins (v_{max}1512 cm^{-1}) modifies the shape of the peak of amide II that consequently shifts from v_{max}1540 cm^{-1} in the spectra of CTRL to v_{max}1530 cm^{-1} wnrs in the spectra of apoptotic cells. Sometimes cells undergoing apoptosis show more pronounced absorbance values at v_{max}1740 cm^{-1} mainly reflecting the increased CO stretching in membrane phospholipids.

We assumed that the spectral features of viable and apoptotic cells could reflect drug-resistance and drug-sensitivity in Ba/F3 cells and mutants exposed to TKIs, respectively.

Unsupervised pattern recognition by HCA

Fig. 2 illustrates the results obtained with the application of unsupervised HCA to individual SR FTIR spectra of Ba/F3 cells within the 1760-1480 cm^{-1} interval of wnrs (Fig. 2A). The representative IR patterns of viable untreated CTRLs (blue) and of Ba/F3 cells and mutants with IR patterns of drug-sensitivity (SENS) and drug-resistance (RES) in samples exposed for 24 and 48 hours to 16.0 nM DAS (pink) or to 2.0 µM IMA (red) are shown in Fig. 2B, respectively. The results of a representative experiment of FC analysis to quantify the relative percentages of viable (V) and apoptotic (EA and A) Ba/F3 cells in samples are shown in Fig. 2C.

wt-Ba/F3 cells

In the dendrogram of 24 hours cell treatment HCA groups in the first class the spectra of 2% DAS- and of 2% IMA-treated cells (pink and red, respectively) together with the spectra of 98% untreated CTRL (blue). The second class contains the spectra of 2% untreated CTRL (blue), 98% DAS-treated (pink) and 98% IMA-treated (red) cells, respectively. These two final classes have a distance of 26.1. In the dataset of cells exposed for 48 hours to TKIs, HCA classifies the spectra of 99% untreated CTRL, 1% DAS and 1% IMA-treated cells in the first class, and of 1% untreated CTRL, 99% DAS-treated and 99% IMA-treated cells in the second class, respectively. The distance between the two classes results 44.6. As compared to the representative average spectra of CTRL wt-Ba/F3 cells (blue traces), the average spectra of DAS- and IMA-treated Ba/F3 cells grouped by HCA show the typical IR pattern of apoptotic cells with IR signatures that can be easily identified in the corresponding second derivative spectra (Fig. 2B pink and red traces, respectively). The percentages of viable and apoptotic cells identified by FC analysis (Fig. 2C) were in agreement with those of HCA.

V299L-Ba/F3 cells

Most spectra of V299L-Ba/F3 cells exposed for 24 and 48 hours to DAS (Fig. 2A, pink traces) are grouped by HCA with those of corresponding untreated CTRLs (blue) and their spectra have very similar IR patterns (Fig. 2B, pink and blue traces, respectively). On the contrary, the spectra of V299L-Ba/F3 cells exposed for 24 and 48 hours to 2.0 µM IMA are mostly grouped by HCA in distinct classes. Typical IR markers of cell apoptosis are not present in the representative spectra of DAS-treated V299L-Ba/F3 cells resulting therefore with an IR pattern of resistance (RES) to the pro-apoptotic action of this TKI. On the contrary, typical IR markers of cell apoptosis are present in the spectra of V299L-Ba/F3 cells treated with IMA and indicate the sensitivity (SENS) of this mutant cell clone to the actions of this TKI. The results of FC analysis confirmed those of HCA.

T315I-Ba/F3 cells

The spectra of untreated CTRL (blue) and of T315I-Ba/F3 mutant cells treated for 48 hours with 16.0 nM DAS (pink) or 2.0 µM IMA (red) are mixed in the dendrogram of Fig. 2A (57% untreated CTRL, 2% DAS-treated, and 51% IMA-treated T315I-Ba/F3 cells spectra in the first class and 43% untreated CTRL, 98% DAS-treated, and 90% IMA-treated T315I-Ba/F3 cells spectra in the second class, respectively). Similar results were obtained in the dataset of spectra of T315-Ba/F3 cells exposed for 24 hours to TKIs. According to their double drug-resistance, the representative spectra of T325I-Ba/F3 cells classified by HCA have no IR pattern of cell apoptosis (Fig. 2B) and only a few apoptotic cells stain for Annexin-V (Fig. 2C).

Significant numbers of apoptotic cells (>15%) could be observed in samples of par- and T315I-Ba/F3 cells exposed for 48 hours to 32 nM DAS and 8.0 µM IMA, respectively. Cumulative fractions of drug-resistant and drug-sensitive Ba/F3 cells and mutants calculated by SR microFTIR+HCA within replicate experiments are shown in ESI Fig. S2.

Supervised identification of IR signatures of TKIs interference with protein phosphorylation processes

TKI treatment induces not only cell apoptosis but also the inhibition of TK activity in sensitive cells. The identification of signatures related to the interferences with abnormal TK activity can therefore represent a valuable tool useful for the early identification of drug-sensitivity/resistance in leukemic blasts.

Fig. 3 illustrates the strategy we used to identify and cross-validate IR markers of protein phosphorylation in Ba/F3 cells. The intensity of phosphate signals reflected by the mean values of integral with limits 1150-900 cm^{-1} in the representative IR spectra was related to the expression/activity of Bcr-Abl and to the degrees of protein tyrosine phosphorylation measured in Ba/F3 cells and mutants with the different levels of sensitivity to the inhibitory actions of IMA and DAS (Fig. 3, A through D, respectively). To associate the absorbance of phosphorylated proteins with specific wnrs, we compared the FTIR absorbance spectra of equimolar samples of purified bovine serum albumin (BSA) which is not a phosphorylated protein, and of ovalbumin (OVA) and non fat milk (NFM) which contain various degrees of phosphate rich proteins such as ovalbumin and caseins, respectively. The spectra of Fig. 3E show absorbance peaks of different intensity within the 1150-700 cm^{-1} interval of wnrs among samples. In particular, NFM has the highest and BSA the lowest absorbance values at v_{max}1070 cm^{-1}, respectively. Therefore we assumed that changes in intensity of the signals within this interval could reflect the different content/degrees of

Journal Name
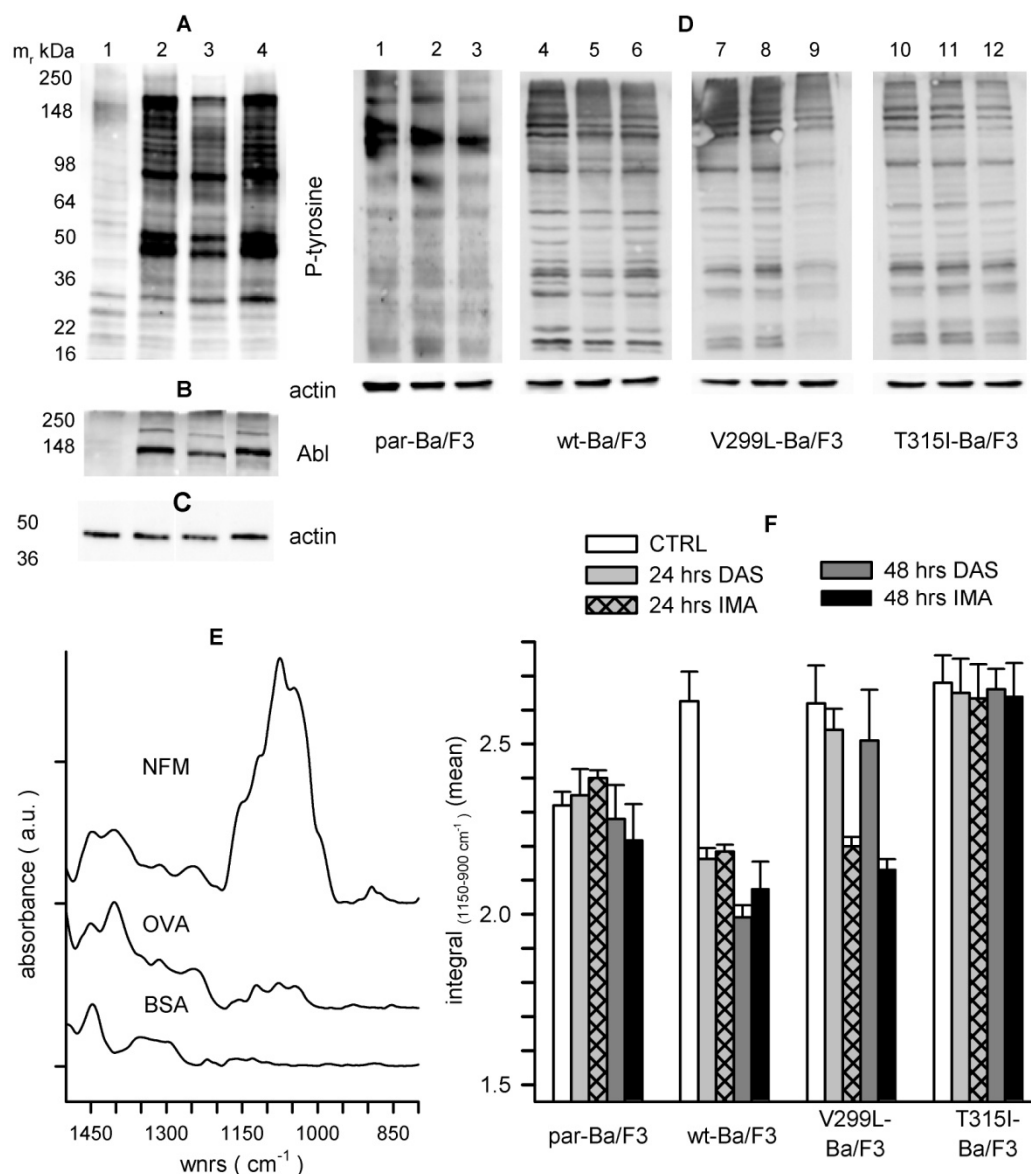
Analyst

ARTICLE TYPE

Fig. 3 Signatures of drug interference with protein phsophorylation processes in Ba/F3 cells and mutants exposed to specific Bcr-Abl tyrosine kinase inhibitors dasatinib (DAS) and imatinib mesylate (IMA). A-C. Immunoblotting analyses in the cell lysates (20 µL/lane adjusted to 1.0 mg total protein mL^{-1}) of untreated CTRL Ba/F3 cells. A-C. lanes 1 through 4: proteins of untreated CTRL parental- (1), wild type-(2), V299L-(3), and T315I-(4) Ba/F3
5   cells probed with a mixture of anti-phosphotyrosine antibodies (A), anti-Abl antibody to confirm the absence/presence of Bcr-Abl (B), and anti-actin antibody (C), respectively. D. Immunoblotting of phosphotyrosine (P-tyrosine) in the lysates of Ba/F3 cells exposed for 24 hours to 16.0 nM DAS or 2.0 µM IMA, respectively. Untreated CTRL: lanes: 1, 4, 7, and 10; Ba/F3 cells exposed to DAS: 2, 5, 8, and 11 or to IMA: 3, 6, 9, and 12, respectively. E. FTIR absorbance spectra of 1.0 mM bovine serum albumin (BSA), ovalbumin (OVA), and non fat milk (NFM) pure reference substances used to identify IR signals from phosphoproteins within the 1500-800 cm^{-1} interval of wnrs. F. The comparison of mean (and error) values of integral with limits 1150-900
10   cm^{-1} calculated in the FTIR absorbance spectra of untreated CTRLs and in par-, wt-, V299L-, and T315I-Ba/F3 cell replicates (n = 3) exposed to TKIs.

phosphorylated proteins in CML cells.[28,34,35]

   To test whether changes within this spectral region were in agreement with the inhibitory actions of IMA and DAS on Bcr-Abl associated TK activity we compared the mean values of
15   integral with limits 1150-900 cm^{-1} in the FTIR absorbance

spectra of untreated control (CTRL) and of Ba/F3 cells replicates exposed to 16.0 nM DAS or 2.0 µM IMA for 24 or 48 hours, respectively. In Fig. 3F significant differences (mean and standard deviation, SD) are observed among untreated CTRL
20   Ba/F3 cells and among parental- and wt-Ba/F3 cells, and V299L-

and T315I-Ba/F3 cell mutants exposed to drugs. In particular the values of this integral reflect those of phosphotyrosine determined by immunoblotting analyses shown in Fig. 3D. The one way analysis of variance, ANOVA carried out in 3 replicate experiments and 2 time points, revealed that the mean values of this integral were significantly lower in untreated CTRL par-Ba/F3 cells (2.32 ± 0.035, n = 6; P< 0.001) as compared with CTRL wt- (2.63 ± 0.07), V299L- (2.62 ± 0.11), and T315I-Ba/F3 cells (2.68 ± 0.08), respectively. Moreover, as compared to corresponding untreated CTRLs the mean values of this integral were significantly reduced in wt-Ba/F3 cells exposed for 24 and 48 hours to DAS (2.16 ± 0.03 and 1.99 ± 0.04; P<0.001) or IMA (2.18 ± 0.12 and 2.08 ± 0.05; P=0.005) and in V299L-Ba/F3 cells exposed to IMA (2.2 ± 0.03 and 2.13 ± 0.03; P=0.04) but not to DAS (2.54 ± 0.06 and 2.51 ± 0.14). According to their double resistance, the values of this integral did not change significantly in the spectra of DAS- and IMA-resistant T315I-Ba/F3 cells. No significant difference was observed also in Bcr-Abl negative par-Ba/F3 cells.
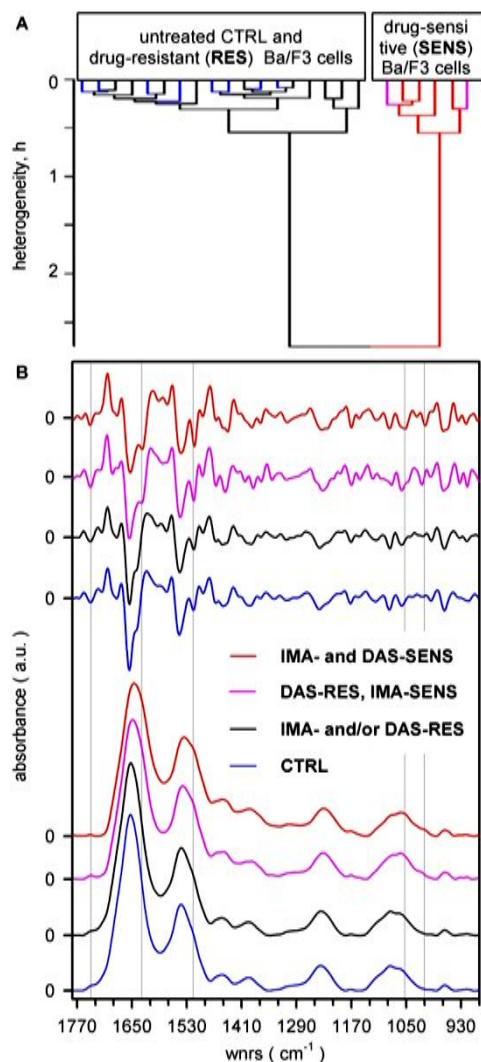

Fig. 4 The unsupervised identification of drug-resistance/sensitivity in samples analysed by microFTIR with globar. A. HCA of 24 average spectra. B. Spectral differences between drug-resistant (black) and drug-sensitive (pink and red) samples have been highlighted with gray lines.

HCA in the spectra obtained by microFTIR with Gobar

Fig.4 illustrates the performance of HCA in classifying drug-sensitive and drug-resistant samples within a dataset of spectra acquired by microFTIR with globar. In the dendrogram of Fig. 4A, 18 spectra are grouped in the first class, included all untreated CTRLs (n=8, blue), all par- and T315I-Ba/F3 treated cells (n=8, black), and DAS-treated V299L-Ba/F3 cells (n=2, black), respectively. Of the remaining 6 spectra grouped in the second class, 4 are those of drug-sensitive wt-Ba/F3 cells exposed for 24 and 48 hours to 16.0 nM DAS or 2.0 µM IMA (red), and 2 are of V299L-Ba/F3 cells exposed to IMA for 24 and 48 hours (pink), respectively. The resulting spectra with IR patterns of drug-resistance and drug-sensitivity are shown in Fig. 4B with major differences highlighted by grey lines. As compared to the spectra of CTRL (blue) and drug-resistant Ba/F3 cells (black) samples that were grouped together by HCA, the spectra of DAS-(pink) and IMA-(red) sensitive samples show typical IR markers of cell apoptosis within the 1760-1480 cm^{-1} interval and additional changes within the 1140-990 cm^{-1} interval or wnrs. In particular, changes at v_{max} 1056 cm^{-1} (CH$_2$OH groups) and at v_{max}1020 cm^{-1} (COH groups) can suggest some interferences of drugs with the metabolism of carbohydrates, respectively.
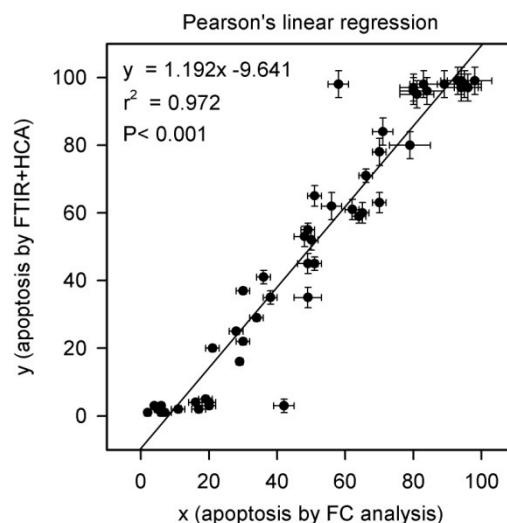

Fig. 5 Correlation observed among data obtained with two independent methods, SR microFTIR+HCA (y) and FC (x), measuring cell apoptosis in samples (means and errors of triplicates).

Correlation studies

The results of correlations studies carried out to evaluate whether two independent methods give concordant information are shown in Fig. 5. The dot-plot correlates cell apoptosis quantified in samples by SR microFTIR+HCA (y) and by FC analysis (x), respectively. A direct and significant linear correlation was calculated (n = 50, Pearson's correlation coefficient = 0.97) and the line describes the following linear regression equation through data points: y = 1.193x - 9.671.

Discussion

The identification of reliable markers of metabolic processes occurring in cells is critical in the field of cell biology and has potential applications in drug discovery and translational

medicine. Since the mid-IR spectrum of a cell reflects whole cell biochemistry, microFTIR absorbance spectroscopy is considered a sensitive analytical technique to obtain complete and rapid information on the whole …*omics* of cell processes.[14,15] The possibility to identify spectral changes reflecting the interference of drugs in cells might suggest the use of mid-IR spectrum as an useful biomarker.[43,44]

Although major differences observed among the spectra in Fig. 1 can immediately suggest the presence of drug resistant samples, the interpretation of subtle differences cannot be obtained by the simple visual inspection and appropriate qualitative and quantitative analyses are required. The acceptable S/N values achieved in the spectra obtained with both SR and globar configurations allowed to perform unsupervised classification by HCA.[17,45] Major advantage of combining mathematical and statistical methods for multivariate analysis is the suppression of subjective component to obtain information on drug-resistance/sensitivity in samples. Therefore, the results of present work have demonstrated that the same accurate identification of drug-sensitive and drug-resistant cells can be obtained by SR microFTIR+HCA (Figs. 2) and, although at lower spatial resolution, also by microFTIR performed with globar (Fig. 4) which is the IR source of first choice for routine microFTIR analyses in samples with benchtop instrumentation. MicroFTIR performed with the highest brilliance SR should be preferentially used for validation of reference spectra.[43]

The possibility to combine microFTIR and computational approach can have several advantages toward classic biochemical and immunochemical approaches that are characterized by more complex manipulations in the samples. No particular skill and minimal manipulation required to prepare samples for microFTIR analysis reduces the probability of introducing artefacts that can influence the final results. Further advantages derive from the reduction of costly reagents like monoclonal antibodies that are extensively used to interrogate the dynamics of cell signalling or the functional status in cells. The potentially high-processivity of microFTIR performed with benchtop instrumentation opens the way to high-throughput screening and further reduction of the costs of individual assays. All these applications, however, rely on the association of IR markers with specific biochemical processes within cells. This implies the initial application of rigorous cross-validation procedures in order to associate specific changes in the IR spectra to a unique or limited set of biochemical, structural, and functional cellular events.

The results of IR analysis in the Ba/F3 cells model of human CML are in agreement with our previous findings obtained in human *BCR-ABL* positive cell lines exposed to TKIs.[28] Moreover, the typical IR signatures of cell apoptosis in Ba/F3 cells and mutants that were sensitive to the actions of TKIs are the same that have been already reported in different cell lines.[36-42] Not only we have quantified cell apoptosis in samples by SR microFTIR+HCA but also we made the cross-validation of IR signatures to use as potential references in future pre-clinical and clinical applications.

The IR spectra of purified molecules or of their mixtures have been already used to assign vibrational components by a supervised frequency approach in the analysis of IR spectra.[34,46] As the dynamic of cellular phosphorylation events are crucial to control cell signalling we have focused part of our efforts on this aspect. Using appropriate cellular models suited for the purpose we were able to unequivocally associate and cross-validate some modification within the phosphate region of mid-IR spectrum to a specific biochemical event involving protein tyrosine phosphorylation (Fig. 3). Another important aspect concerns with the capability to measure apoptotic/necrotic events associated to the effectiveness of drugs used. Several drug screening protocols rely on these parameters to select drug candidates to move forward toward the drug-discovery pipeline. For example, National Cancer Institute protocols for the preliminary *in vitro* screening expose three human cancer cell lines to a single dose of new drug for 48 hours. If the growth of one or more cell lines is inhibited, the drug is then probed against the full panel of 60 human cancers. Only 2% of approximately 2,500 compounds tested on a yearly basis usually progress to the next stage of testing in mice (http://www.cancer.gov/cancertopics/factsheet/NCI/drugdiscover y). It is evident that any improvement can bring to higher throughput and has an impact into making more cost/effective this approach as a drug-screening program.

The results of present study suggest that two critical parameters of interest in drug screening/testing can be evaluated within the IR spectrum: cell death and the levels of phosphorylation in proteins. As the mid-IR spectrum can reveal both events, microFTIR performed in samples subjected to a simple processing and within a single round of measurement appears an advantageous approach in comparison with analytical methods that evaluate only one of these parameters at the time (typically cell proliferation/death). Furthermore, such events can be evaluated at the single-cell level or at a wider cell population level according to the instrument setting chosen.

Conclusions

The microFTIR+HCA approach as described in the present paper is well suited for a drug screening program based on the identification of TKI/Phosphatase activators. Being able to identify also signature of cell death, it can be applied to a much wider range of compounds and cellular models of disease. Since microFTIR analysis does not damage the sample, and the measurement can be performed on formalin-fixed then dried cells, there is no room for cell alteration after drug treatment. Therefore, samples can also be sent to different facilities/labs for multi-centric evaluation and protocols standardization.

In conlcusion, this combined microFTIR+HCA approach requiring minimal sample handling potentially represents a convenient and more robust screening approach to identify drug-resistance/sensitivity in leukemic cell lines as well as in leukemic blasts from peripheral blood of patients.

Acknowledgements

Addresses

[a] *Azienda Ospedaliera Universitaria Integrata Verona, Department of Pathology and Diagnostics - Unit of Immunology, Policlinico G. Rossi, P.le L.A. Scuro, 10, I-37134, Italy.* Fax: +390458027127; Tel: +390458027552; E-mail: giuseppe.bellisola@univr.it

[b] *University of Verona, Department of Pathology and Diagnostics – General Pathology, Strada Le Grazie, 8, I-37134, Verona, Italy.* Fax: +390458027127; Tel: +390458027688; E-mail: claudio.sorio@univr.it ; marzia.vezzalini@univr.it ; elisabetta.moratti@univr.it ; giovannino.silvestri@univr.it

[c] *Diamond Light Source Ltd, Diamond House, Harwell Science and Innovation Campus, Didcot, Oxfordshire, United Kingdom.* Tel: +441235778410; E-mail: gianfelice.cinque@diamond.ac.uk; katia.wehbe@diamond.ac.uk

[d] *University of Milano-Bicocca, Department of Clinical Medicine and Prevention, Via Cadore, 48, I-20052 Monza, Monza Brianza, Italy.* Fax: +390392333539; Tel: +3903964488362; E-mail: sara.redaelli@unimib.it; carlo.gambacorti@unimib.it

* *These authors share first authorship.*

† Electronic Supplementary Information (ESI) available:
Fig. S1. The optimisation of microFTIR analysis in samples. Two spectra of the same individual cell restricted by 15x15 μm² aperture slits were obtained by microFTIR performed consecutively with synchrotron radiation (SR) and globar as the external and internal IR sources, respectively. The significantly different signal to noise (S/N) values achieved in each spectrum within the 2600-2400 cm⁻¹ interval of wavenumbers (wnrs) have been reported. To improve the quality of spectra acquired with globar, the aperture slits were set to 50x50 μm² and IR signals were collected from larger areas over homogeneous zones within samples. Spectra with similar quality were obtained by microFTIR with SR and globar within the 1300-900 cm⁻¹ interval of wnrs allowing to apply algorithms for unsupervised pattern recognition to a wide interval of wnrs. See DOI: 10.1039/b000000x/

Fig. S2. Cumulative fractions of drug-resistant (blue bars) and drug-sensitive (pink and red bars) cells identified by SR microFTIR+HCA in samples (mean of 3 independent experiments). See DOI: 10.1039/b000000x/

‡ Most data have been presented at the Synchrotron User Meeting 2012, workshop Cell Microbiology: form cancer research to stem cells; 5-6 September 2012, Diamond Light Source, Chilton, Oxfordshire, UK.

References

1   T. O'Hare, M.W. Deininger, C.A. Eide, T. Clackson and B.J. Druker, *Clin. Cancer Res.*, 2011;**17**, 212-221.
2   B.J. Druker, *Blood*, 2008, **112**, 4808-4817.
3   S. Roychowdhury and M. Talpaz, *Blood Rev.*, 2010, **25**, 279-290.
4   L.J. Lombardo, F.Y. Lee, P. Chen, D. Norris, J.C. Barrish, K. Behnia, S. Castaneda, L.A. Cornelius, J. Das, A.M. Doweyko, C. Fairchild, J.T. Hunt, I. Inigo, K. Johnston, A. Kamath, D. Kan, H. Klei, P. Marathe, S. Pang, R. Peterson, S. Pitt, G.L. Schieven, R.J. Schmidt, J. Tokarski, M.L. Wen, J. Wityak and R.M. Borzilleri, *J. Med. Chem.*, 2004, **47**, 6658-6661.
5   E. Weisberg, P.W. Manley, W. Breitenstein, J. Brüggen, S.W. Cowan-Jacob, A. Ray, B. Huntly, D. Fabbro, G. Fendrich, E. Hall-Meyers, A.L. Kung, J. Mestan, G.Q. Daley, L. Callahan, L. Catley, C. Cavazza, M. Azam, D. Neuberg, R.D. Wright, D.G. Gilliland and J.D. Griffin, *Cancer Cell*, 2005, **7**, 129-141.
6   L.L. Remsing Rix, U. Rix, J. Colinge, O. Hantschel, K.L. Bennett, T. Stranzl, A. Müller, C. Baumgartner, P. Valent, M. Augustin, J.H. Till and G. Superti-Furga, *Leukemia*, 2009, **23**, 477-485.
7   N.P. Shah, *Clin. Adv. Hematol. Oncol.*, 2011, **9**, 925-926.
8   C.A. Eide, L.T. Adrian, J.W. Tyner, M. Mac Partlin, D.J. Anderson, S.C. Wise, B.D. Smith, P.A. Petillo, D.L. Flynn, M.W. Deininger, T. O'Hare and B.J. Druker, *Cancer Res.*, 2011,71, 3189-3195.
9   B. Mitchell and M. Deininger, *Leuk. Lymphoma*, 2011, **52 Suppl 1**, 4-11.
10 G. Gerrard, K. Mudge, P. Foskett, D. Stevens, M. Alikian, H.E. White, N.C. Cross, J. Apperley and L Foroni, *Am. J. Hematol.*, 2012, **87**, 717-720.
11 P. La Rosée, S. Holm-Eriksen, H. Konig, N. Härtel, T. Ernst, J. Debatin, M.C. Mueller, P. Erben, A. Binckebanck, L. Wunderle, Y. Shou, M. Dugan, R. Hehlmann, O.G. Ottmann and A. Hochhaus, *Haematologica*, 2008, **93**, 765-769.
12 S. Soverini, A. Hochhaus, F.E. Nicolini, F. Gruber, T. Lange, G. Saglio, F. Pane, M.C. Müller, T. Ernst, G. Rosti, K. Porkka, M. Baccarani, N.C. Cross and G. Martinelli, *Blood*, 2011, **118**, 1208-1215.
13 S.K. McWeeney, L.C. Pemberton, M.M. Loriaux, K. Vartanian, S.G. Willis, G. Yochum, B. Wilmot, Y. Turpaz, R. Pillai, B.J. Druker, J.L. Snead, M. MacPartlin, S.G. O'Brien, J.V. Melo, T. Lange, C.A. Harrington and M.W. Deininger, *Blood*, 2010, **115**, 315-325.
14 L. Quaroni and T. Zlateva, *Analyst*, 2011, **136**, 3219-3232.
15 L.M. Miller and P. Dumas, *Curr. Opin. Struct. Biol.*, 2010 , 20, 649-656.
16 J. Trevisan, P.P. Angelov, P.L. Carmichael, A.D. Scott and F.L. Martin, *Analyst*, 2012, **137**, 3202-3215.
17 R. Bhargava, *Anal. Bioanal. Chem.*, 2007, **389**, 1155-1169.
18 K.Z. Liu, M. Xu and D.A. Scott, *Br. J. Haematol.*, 2007, **136**, 713-722.
19 J. Babrah, K. McCarthy, R.J. Lush, A.D. Rye, C. Bessant and N. Stone, *Analyst*, 2009, **134**, 763-768.
20 A. Derenne, M. Verdonck and E. Goormaghtigh. *Analyst*, 2012, **137**, 3255-3264.
21 F. Draux, P. Jeannesson, C. Gobinet, J. Sule-Suso, J. Pijanka, C. Sandt, P. Dumas, M. Manfait and G.D. Sockalingum, *Anal. Bioanal. Chem.*, 2009, **395**, 2293-2301.
22 R. Gasper, J. Dewelle, R. Kiss, T. Mijatovic and E. Goormaghtigh, *Biochim. Biophys. Acta.*, 2009, **1788**, 1263-1270.
23 C.M. Krishna, G. Kegelaer, I. Adt, S. Rubin, V.B. Kartha, M. Manfait and G.D. Sockalingum, *Biopolymers*, 2006, **82**, 462-470.
24 S. Redaelli, R. Piazza, R. Rostagno, V. Magistroni, P. Perini, M. Marega, C .Gambacorti-Passerini and F. Boschelli, *J. Clin. Oncol.*, 2009, **27**, 469-471.
25 R. Palacios, G. Henson, M. Steinmetz and J.P. McKearn, *Nature*, 1984, **309**, 126-131.
26 P.W. Manley, S.W. Cowan-Jacob, E. Buchdunger, D. Fabbro, G. Fendrich, P. Furet, T. Meyer and J. Zimmermann, *Eur. J. Cancer*, 2002, **38 Suppl 5**, S19-S27.
27 J.S. Tokarski, J.A. Newitt, C.Y. Chang, J.D. Cheng, M. Wittekind, S.E. Kiefer, K. Kish, F.Y. Lee, R. Borzillerri, L.J. Lombardo, D. Xie, Y. Zhang and H.E. Klei, *Cancer Res.*, 2006, **66**, 5790-5797.
28 G. Bellisola, M. Della Peruta, M. Vezzalini, E. Moratti, L. Vaccari, G. Birarda, M. Piccinini, G. Cinque and C. Sorio, *Analyst*, 2010, **135**, 3077-3086.
29. G. Cinque, M. Frogley, K. Wehbe, J. Filik and J. Pijanka, *Synchrotron Radiation News*, 2011, DOI: 10.1080/08940886.2011.618093

30 P. Lasch and W. Petrich, in *Biomedical Applications of Synchrotron Infrared Microspectroscopy. A Practical Approach*, ed. D. Moss, RSC Publishing, Cambridge, 2010, ch. 6, pp. 192-225.

31 L. Wang and B. Mizaikoff, *Anal.Bioanal. Chem.*, 2008, **391**, 1641-1654.

32 B. Lavine and J. Workman, *Anal. Chem.*, 2010, **82**, 4699-4711.

33 A. Barth, *Biochim. Biophys. Acta*, 2007, **1767**,1073-1101.

34 M. Diem, S. Boydston-White and L. Chiriboga, *Applied Spectroscopy*, 1999, **53**, 148a-151a.

35 I. Yousef, J. Bréard, N. Sid Ahmed-Adrar, A. Maâmer-Azzabi, C. Marchal, P. Dumas, F. Le Naour, *Analyst*, 2011, **136**, 5162-5168.

36 H.Y. Holman, M.C. Martin, E.A. Blakely, K. Bjornstad and W.R. McKinney, *Biopolymers*, 2000, **57**, 329-335.

37 K.Z. Liu, L. Jia, S.M. Kelsey, A.C. Newland and H.H. Mantsch, *Apoptosis*, 2001, **6**, 269-278.

38 F. Gasparri and M. Muzio, *Biochem. J.*, 2003, **369(Pt 2)**, 239-248.

39 N. Jamin, L. Miller, J. Moncuit, W.H. Fridman, P. Dumas and J.L. Teillaud, *Biopolymers*, 2003, **72**, 366-373.

40 U. Zelig, J. Kapelushnik, R. Moreh, S. Mordechai and I. Nathan, *Biophys. J.*, 2009, **97**, 2107-2114.

41 L. Di Giambattista, D. Pozzi, P. Grimaldi, S. Gaudenzi, S. Morrone and A.C. Castellano, *Anal. Bioanal. Chem.*, 2011, **399**, 2771-2778.

42 S. Machana, N. Weerapreeyakul, S. Barusrux, K. Thumanu and W. Tanthanuch, *Talanta*, 2012, **93**, 371-382.

43 G. Bellisola and C. Sorio, *Am. J. Cancer Res.*, 2012, **2**, 1-21.

44 L.B. Mostaco-Guidolin and L. Bachmann, *Applied Spectroscopy Reviews*, 2011, **46**, 388-404.

45 P. Lasch and D. Naumann, Biochim. Biophys. Acta, 2006, **1758**, 814-829.

46 E. Benedetti, E. Bramanti, F. Papineschi, I. Rossi and E. Benedetti, *Applied Spectroscopy*, 1997, **51**, 792-797.
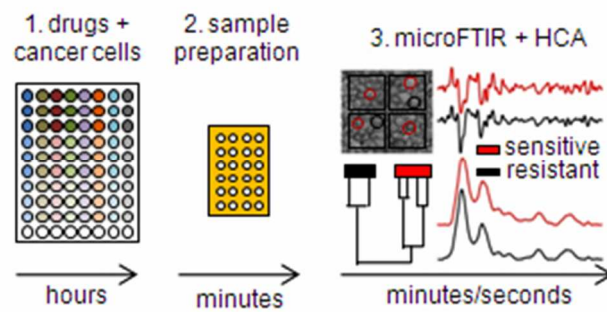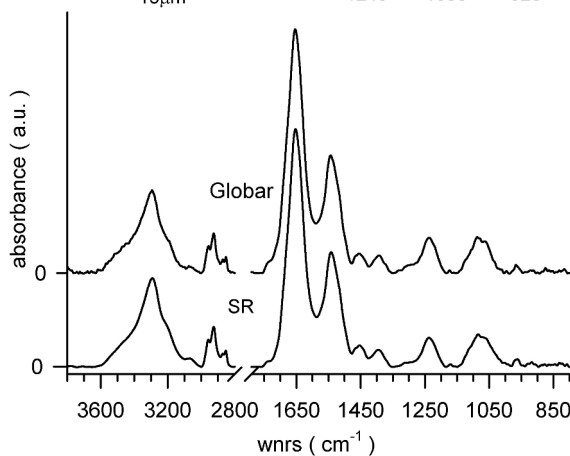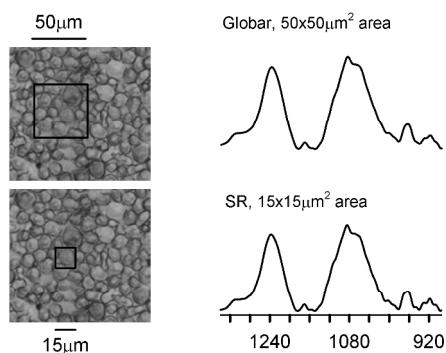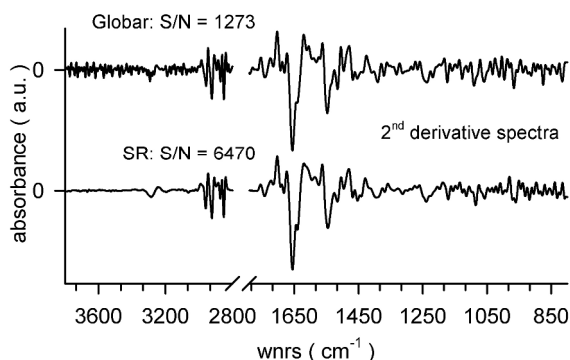
Fourier Transform InfraRed microspectroscopy (microFTIR) in combination with unsupervised Hierarchical Cluster Analysis (HCA) is a rapid, robust, and relatively inexpensive method suitable for high-throughput identification and classification of drug-sensitivity/-resistance in leukemic cells.
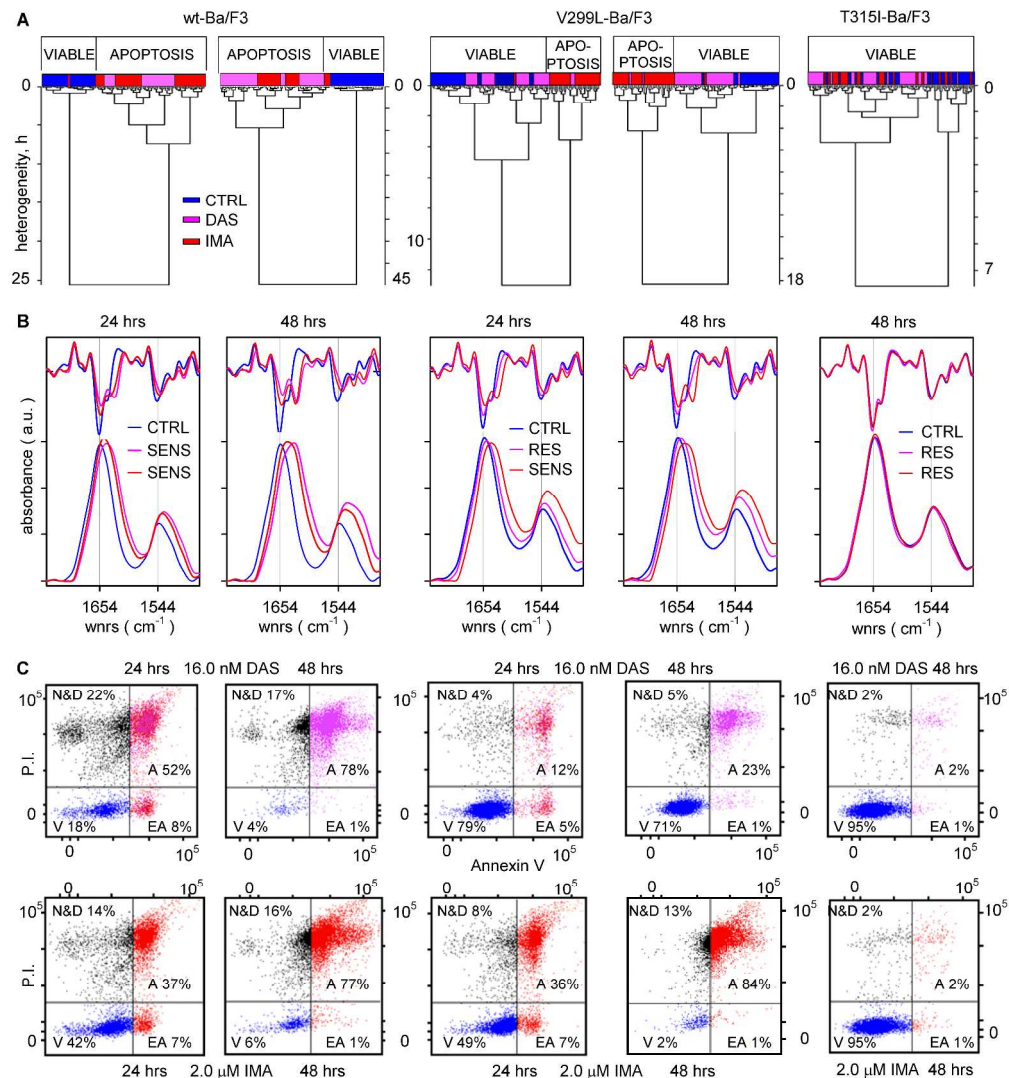56x28mm (144 x 144 DPI)
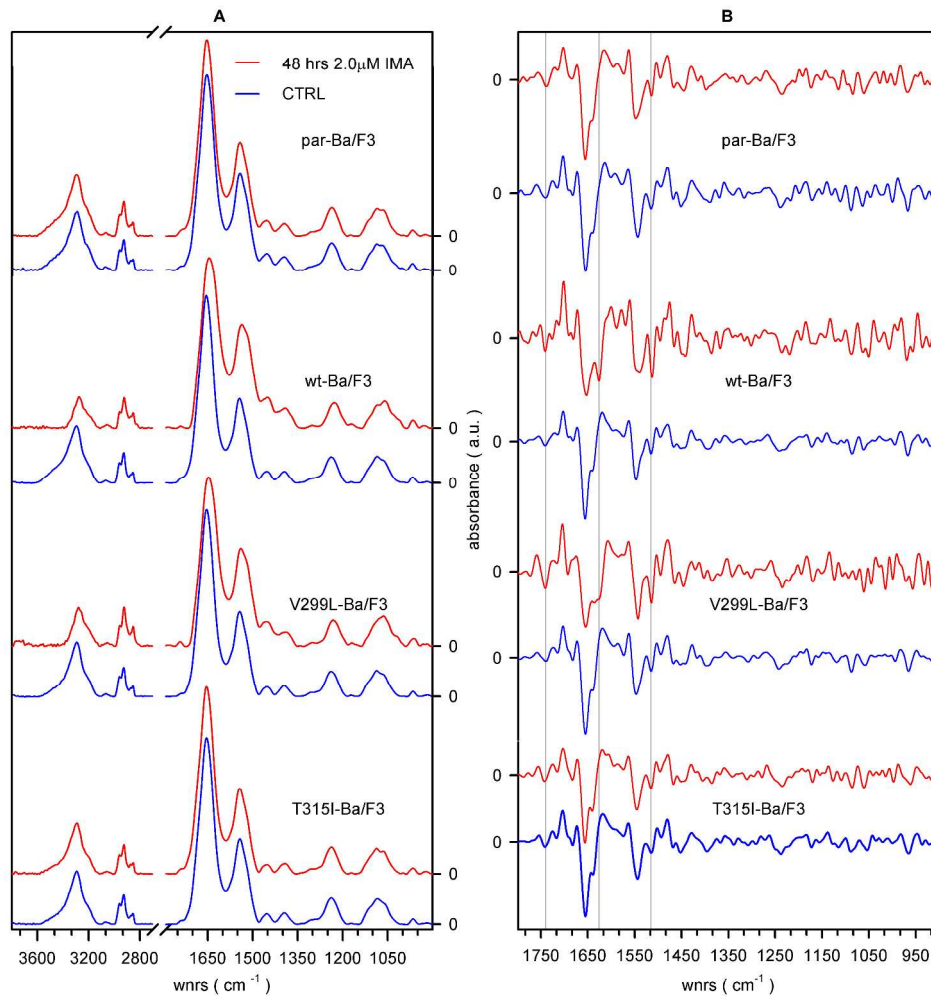
Supervised analyses in the representative FTIR absorbance spectra of mouse-derived Ba/F3 cells model of human chronic myeloid leukemia (CML). A. Normalized and baseline corrected spectra are shown within the 3800-800 cm-1 interval of wnrs (omitted 2700-1800 cm-1 interval). Blue traces: untreated control (CTRL); red traces: samples exposed to 2.0 µM imatinib mesylate (IMA) for 48 hours. B. The corresponding second order derivative spectra within the 1800-900 cm-1 interval. Typical IR signatures of cell apoptosis induced by IMA have been marked with grey lines.
641x665mm (150 x 150 DPI)

The optimisation of microFTIR analysis in samples. Two spectra of the same individual cell restricted by 15x15 µm2 aperture slits were obtained by microFTIR performed consecutively with synchrotron radiation (SR) and globar as the external and internal IR sources, respectively. The significantly different signal to noise (S/N) values achieved in each spectrum within the 2600-2400 cm-1 interval of wavenumbers (wnrs) have been reported. To improve the quality of spectra acquired with globar, the aperture slits were set to 50x50 µm2 and IR signals were collected from larger areas over homogeneous zones within samples. Spectra with similar quality were obtained by microFTIR with SR and globar within the 1300-900 cm-1 interval of wnrs allowing to apply algorithms for unsupervised pattern recognition to a wide interval of wnrs. 366x717mm (150 x 150 DPI)

Unsupervised recognition of IR patterns by hierarchical cluster analysis (HCA). A. HCA was applied to the 1760-1480 cm-1 interval of SR FTIR absorbance spectra of individual cells in untreated CTRL, and DAS- or IMA-treated (24 or 48 hours) samples of wt-, V299L-, and T315I-Ba/F3 cells (24 hrs has been omitted). B. The representative spectra averaging those of individual cells grouped in each of the two final classes are shown according to the condition of drug treatment: blue, untreated CTRL; pink, 16.0 nm DAS; red, 2.0 μM IMA. The corresponding second derivatives have been superimposed to highlight spectral differences between drug-sensitive (SENS) and drug-resistant (RES) cells as compared to those of untreated CTRL (blue). C. The cross-validation of HCA by flow cytometry (FC). Dot-plots of Annexin-V to Propidium Iodide (P.I.) staining in Ba/F3 cells and mutants exposed to 16.0 nM DAS or 2.0 μM IMA for 24 and 48 hours, respectively. The relative percentages of viable cells (V), of cells in early and late apoptosis (EA, A, respectively), and of necrotic cells and debris (N&D) measured in a typical time-course experiment with drugs have been reported.
784x844mm (150 x 150 DPI)
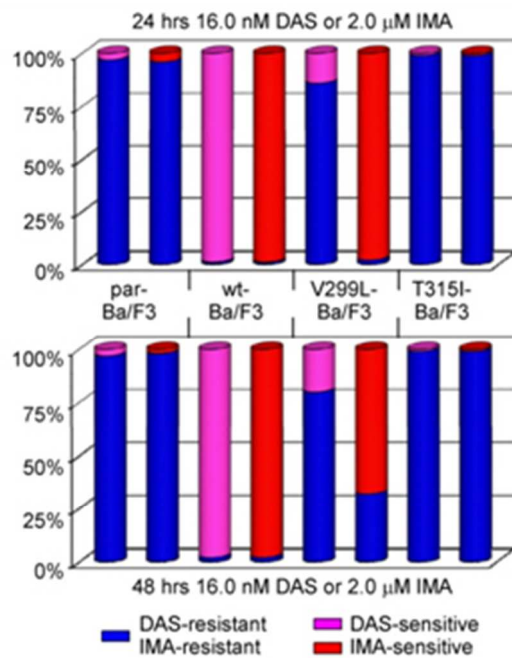
Cumulative fractions of drug-resistant (blue bars) and drug-sensitive (pink and red bars) cells identified by
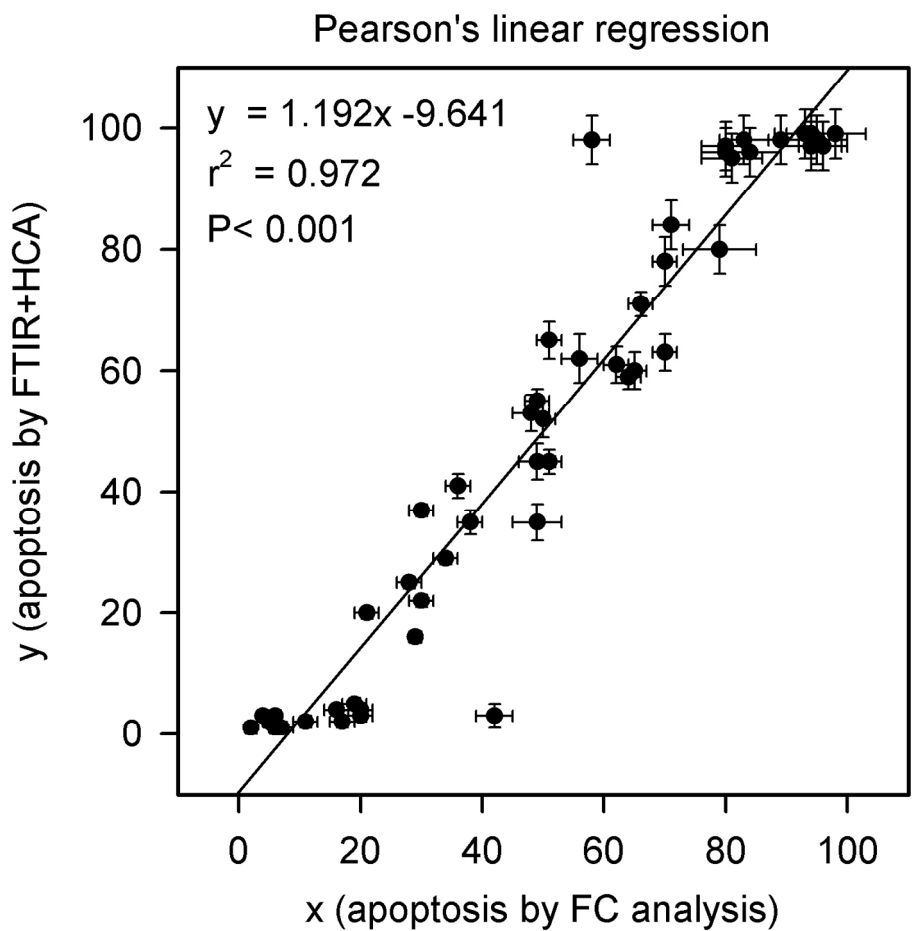SR microFTIR+HCA in samples (mean of 3 independent experiments).
96x118mm (72 x 72 DPI)
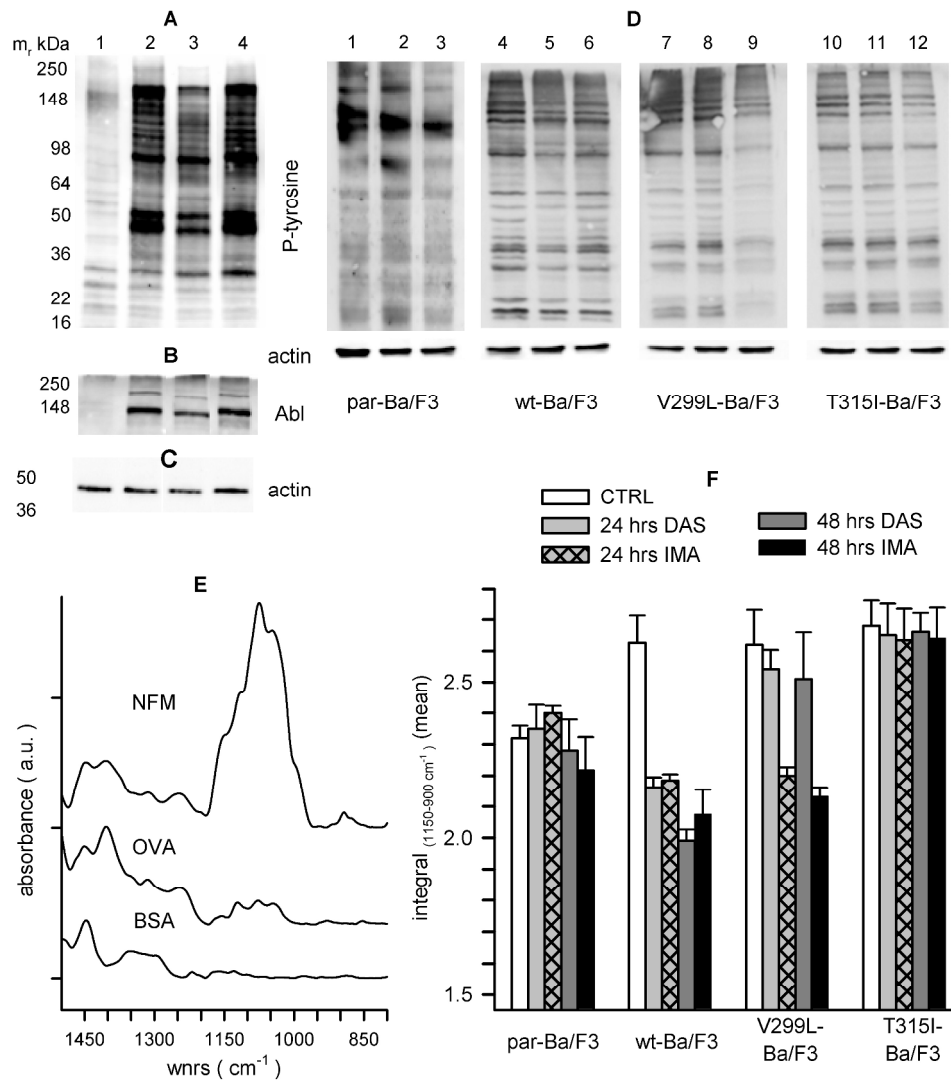
Signatures of drug interference with protein phsophorylation processes in Ba/F3 cells and mutants exposed to specific Bcr-Abl tyrosine kinase inhibitors dasatinib (DAS) and imatinib-mesylate (IMA). A-C. Immunoblotting analyses in the cell lysates (20 µL/lane adjusted to 1.0 mg total protein mL-1) of untreated CTRL Ba/F3 cells. A-C. lanes 1 through 4: proteins of untreated CTRL parental- (1), wild type-(2), V299L-(3), and T315I-(4) Ba/F3 cells probed with a mixture of anti-phosphotyrosine antibodies (A), anti-Abl antibody to confirm the absence/presence of Bcr-Abl (B), and anti-actin antibody (C), respectively. D. Immunoblotting of phosphotyrosine (P-tyrosine) in the lysates of Ba/F3 cells exposed for 24 hours to 16.0 nM DAS or 2.0 µM IMA, respectively. Untreated CTRL: lanes: 1, 4, 7, and 10; Ba/F3 cells exposed to DAS: 2, 5, 8, and 11 or to IMA: 3, 6, 9, and 12, respectively. E. FTIR absorbance spectra of 1.0 mM bovine serum albumin (BSA), ovalbumin (OVA), and non fat milk (NFM) pure reference substances used to identify IR signals from phosphoproteins within the 1500-800 cm-1 interval of wnrs. F. The comparison of mean (and error) values of integral with limits 1150-900 cm-1 calculated in the FTIR absorbance spectra of untreated CTRLs and in par-, wt-, V299L-, and T315I-Ba/F3 cell replicates (n = 3) exposed to TKIs.
599x647mm (150 x 150 DPI)
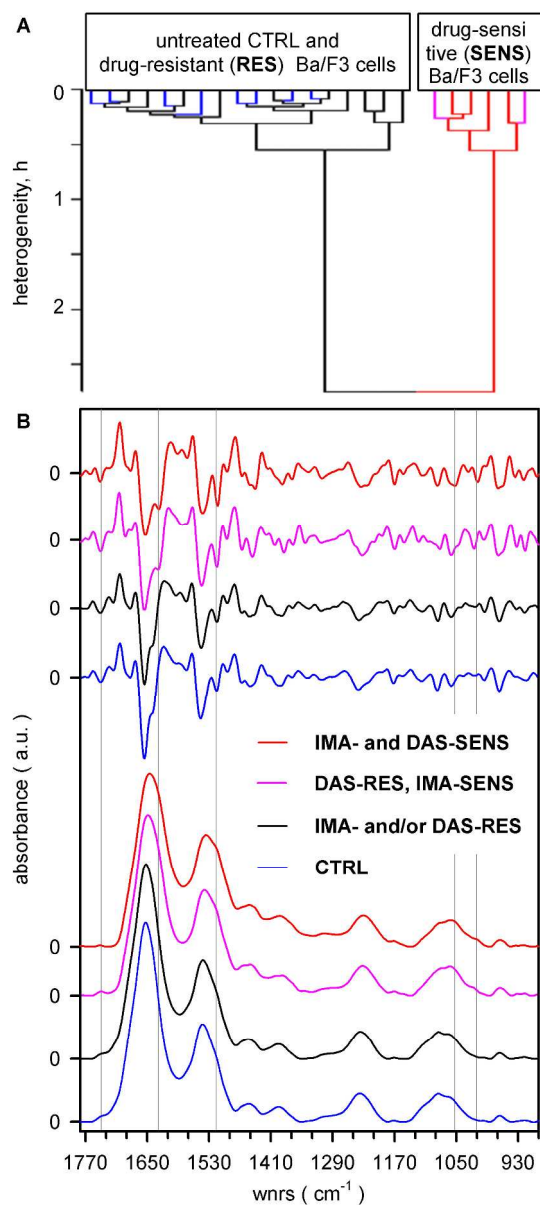
The unsupervised identification of drug-resistance/sensitivity in samples analysed by microFTIR with globar.
A. HCA of 24 average spectra. B. Spectral differences between drug-resistant (black) and drug-sensitive
(pink and red) samples have been highlighted with gray lines.
320x658mm (150 x 150 DPI)

Correlation observed among data obtained with two independent methods, SR microFTIR+HCA (y) and FC (x), measuring cell apoptosis in samples (means and errors of triplicates).
301x289mm (150 x 150 DPI)